

CONTROLLABLE PREPARATION AND DRUG RELEASE BEHAVIOR OF DUAL-LOADED NANOFIBROUS MATS

T. SHAOJIE, G. HUIWEN, G. JING*, W. LU

*Key Laboratory of Textile Science and Technology of Ministry of Education,
College of Textiles Donghua University, Shanghai, China*

Using Chitosan/PEO as the shell and PCL as the core, the effects of electrospinning parameters on the fine control of core-shell structure nanofibers were discussed. Study results showed that the injection velocity ratio of the core solution to the shell solution could influence the core-shell microstructure of the nanofibers closely. Packing the analgesic lidocaine hydrochloride (Lid) in the shell and antibacterial curcumin (Cur) in the core constructed CS-PEO-Lid/PCL-Cur dual-loaded nanofibers. The dual-loaded nanofibers had clear core-shell structure without the drug particles accumulating. The drugs were mainly distributed in the amorphous region of the polymers uniformly. In vitro release tests showed that both the release of Lid and Cur were via Fick diffusion. Drugs release in the different core-shell microstructures exhibited different release ratios. Moreover, a rapid release of Lid and a sustained release of Cur were observed to provide the immediate effects of analgesia and long-term antibacterial activity in the process of wound healing. So the dual-loaded coaxial nanofiber mats with controllable microstructure and sequential drug-release abilities could be a promising wound dressing.

(Received July 1, 2020; Accepted October 13, 2020)

Keywords: Core-shell structure, Dual drug-loaded nanofiber, Sequential drug release, Controlled drug release, Nanofibers

1. Introduction

Because the electrospun membrane has a fibrous structure similar to the extracellular matrix (ECM) [1], many researchers have tried to add substances such as drugs[2-5], enzymes[6], proteins[7,8], and growth factors[9,10] to electrospun fibers for applications in wound dressings, tissue engineering, and controlled release of drugs. Especially in the field of drug controlled release, by using electrospun nanofiber mats as drug carriers, a variety of drug release modes can be achieved including immediate release, delayed release, and sequential release of drugs. There are many ways to achieve the above release modes. One is to attach the drug to the matrix material by post-treatment, including impregnation[11] and grafting[12]. The other method is to prepare drug-loaded fiber mats to add the drug directly to the carrier solution[13] or to select drugs and matrix materials with different hydrophobicities[14,15]. What's more, wrapping the drug in nanoparticles and compounding it with a matrix material to form a drug dressing[16] can achieve a more stable release of the drug.

* Corresponding author: gao2001jing@dhu.edu.cn

Besides, constructing a core-shell system is also a common method to control drug release. At present, the main methods for preparing core-shell nanofibers are emulsion electrospinning and coaxial electrospinning. Emulsion electrospinning uses a simple single-nozzle electrospinning device to prepare core/shell composite nanofibers, and can also achieve the desired slow-release properties[17,18]. However, emulsion electrospinning has high requirements for the spinning solution, and its application is also limited due to the instability of the emulsion. Therefore, coaxial electrospinning technology is more commonly used to construct core-shell structures. The nanofiber membrane prepared by coaxial electrostatic spinning has a unique core-shell structure. It can not only achieve the slow release of drugs by loading the drug in the core layer[19] but also realize the sequential release of two drugs by loading drugs in the core layer and the shell layer simultaneously[20].

The natural polymer material chitosan is a positively charged natural polysaccharide, which can combine negative electrons to promote the adhesion and aggregation of platelets, and has good hemostatic properties for wound bleeding. At the same time, chitosan also has good biocompatibility and is widely used in the field of medical dressings [21]. The research showed that compared with ordinary non-toxic dressings, chitosan film can accelerate wound healing and promote the regeneration of epidermal cells and granular layers[22]. However, it also has the disadvantages of poor spinnability. In addition to improving the properties of chitosan by improving the structure of the chitosan film, chitosan can be prepared by mixing chitosan with other materials, such as polyethylene oxide (PEO) [23]. PCL has hydrophobic properties and is usually used as a drug carrier in the drug delivery system. Besides, for wound dressing applications, PCL is used in the mixture can provide mechanical strength to the dressing[24].

Based on the above studies, we selected CS/PEO and PCL as the shell and core materials, respectively, and put the analgesic Lid and antibacterial Cur into the shell and the nuclear layer respectively. As shown in Fig. 1, dual-drug loaded core-shell nanofibers with the controllable diameter were prepared by coaxial electrospinning technology and explored the differential effect of these diameters on drug release. In the early stages of wound healing, it exerts the hemostatic effect and biocompatibility of chitosan. Furthermore, the initial release rate of analgesics in the shell is high, which can achieve the purpose of rapid analgesia. During the inflammatory phase of the wound, the antibacterial drugs in the nuclear layer continued to be slowly released to achieve the purpose of sustained antibacterial, which fully realized the functional synergy of the dressing and the timing of drug release. This coaxial nanofiber, which adjusts the diameter to control the drug release rate, is expected to be applied in different wound environments.

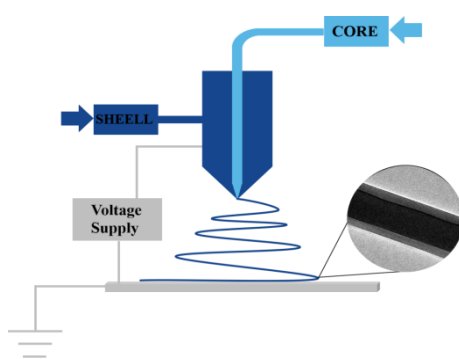


Fig. 1. Schematic illustration of the formation of core-shell structure.

2. Experimental

2.1. Material

Chitosan (degree of deacetylation = 90.6%, Viscosity = 90 mPa.s) was from Zhejiang Golden-Shell Pharmaceutical Co.,Ltd., (China); Polyethylene oxide (PEO, Mw = 1000 kDa) was provided by J&K Chemical Co.,Ltd. (China); Polycaprolactone (PCL, Mw = 8000 g/mol) was purchased from Sigma-Aldrich (China); Lidocaine hydrochloride (Lid) and Curcumin (Cur) were obtained from Sangon Biotech Co., Ltd. (China); Acetic acid (AA), dichloromethane (CH₂CL₂) and N, N-Dimethylformamide (DMF) were supplied by Shanghai Ling Feng Chemical Reagent Co., Ltd. (China). All reagents were analytical grade and used without further purification. Deionized water was used in sample preparation.

2.2. Preparation of drug loaded core-shell nanofibers

At room temperature, a certain amount of CS and PEO (mass ratio 95/5) were dissolved in AA/H₂O (volume ratio 90/10) mixed solution to obtain the non-loaded shell solution (mass fraction 5%). Then add the analgesic drug Lid with mass fraction of 5% dissolved in H₂O to obtain the Lid-loaded shell solution(mass fraction 5%).

A certain amount of PCL was dissolved in DCM/DMF (volume ratio 90/10) mixed solution to get the non-loaded core solution(mass fraction 10%). Then add the antibacterial drug Cur with mass fraction of 5% dissolved in DMF to get the Cur-loaded core solution (mass fraction 10%). All the solutions were sealed and stirred for 12 hours on a magnetic stirrer to obtain homogeneous solutions.

For coaxial electrospinning, the prepared solutions were respectively fed into the stainless steel coaxial needle (Changsha Nayi, China) at flow rates controlled by two syringe pumps. Under the voltage of 15 kV, the receiving distance of 20 cm and the injection speed of core layer of 0.2 mL/h, coaxial electrospinning was performed with the injection velocity ratios of core layer and shell layer at 1:2, 1:4, and 1:6, respectively.

In addition, the core layer solution was separately sucked into a 5 mL medical syringe. Under the voltage of 15 kV, the receiving distance of 20 cm and the injection speed of 0.3 mL/h, The uniaxial nanofibers with Cur loaded were prepare as a control sample.

All electrospinning experiments were conducted at about 25 °C and 20%-30% humidity. After about 6 hours of electrostatic spinning, the nanofibrous mats were dried at ambient conditions for 24h before further analysis.

2.3. Scanning electron microscopy (SEM) analysis.

Scanning electron microscopy (JSM-5600LV, JEOL, Japan) was employed to observe the morphology of the nanofibers. Electrospun nanofibrous mats were mounted onto aluminum foil and coated with gold-palladium. Software Nano measure was used to determine the diameter of the fibers at one hundred different points.

2.4. Transmission electron microscopy (TEM) analysis.

Transmission electron microscopy (H-800, Hitachi, Japan) was employed to confirm the

core-shell structure of the nanofibers. The samples for TEM observation were prepared by spinning onto carbon-coated copper grid for about 10 s.

2.5. Fourier transform infrared spectroscopy (FTIR) analysis.

Fourier transform infrared spectroscopy (Nicolet 6700, Thermo Fisher Scientific Co., Ltd., USA) was used to characterize the chemical structure of nanofibers in the mid-infrared from 4000 to 600 cm^{-1} with a resolution of 2 cm^{-1} .

2.6. X-ray diffraction (XRD) analysis.

X-ray diffraction (D/max-2550PC, Rigaku, Japan) was used to illustrate the crystalline structure of nanofibers in the 2θ range of $5\text{--}60^\circ$ with a scanning speed at $10^\circ/\text{min}$.

2.7. In vitro drugs release analysis

In vitro release of dual-drug-loaded nanofibrous mats was conducted by incubating them (30 mg) in 8 mL phosphate buffered saline ($\text{pH} = 7.4$) at 37°C with constant shaking at 80 rpm. At specified time intervals 1 mL of the release medium was removed for Lid. However, for Cur, appropriate proportion of ethanol had to be added to the release media due to the poor water solubility. Meanwhile, 1 mL fresh phosphate buffered saline was added to the release medium. Then the absorbance of Lid and Cur at 205 nm and 429 nm were achieved using UV-vis spectroscopy. Plot the cumulative release rate against time. At the same time, the drugs release kinetics of were analyzed. All measurements were operated in triplicates, and the results were reported as average values.

2.8. Statistical analysis

To compare the statistical significance of the different samples, one-way analysis of variance (ANOVA) with significant level $p < 0.05$ was used. The data were recorded as mean \pm standard deviation ($n = 3$) and the error bars correspond to one standard deviation in the Fig.s. The data in the Fig.s were marked by an asterisk (*) for $p < 0.05$ and two asterisks (**) for $p < 0.01$.

3. Results and discussion

3.1. Morphology and microstructure of core-shell nanofibers

The morphology of the core-shell nanofibers and the corresponding diameter distributions were shown in Fig. 2. It indicated that the fiber diameters were 260 ± 47 , 390 ± 45 , 443 ± 94 and 457 ± 74 nm when the core-shell injection velocity ratio was 1:1, 1:2, 1:4 and 1:6, respectively. The fiber diameter increased with the increase of the injection velocity ratio, while the fiber unevenness increased first and then decreased. The most likely reason was when the injection velocity of the shell layer accelerated, the solvent could not evaporate in time, making the fibers thicker. As the injection velocity ratio was 1:2, the fiber distribution was the most uniform.

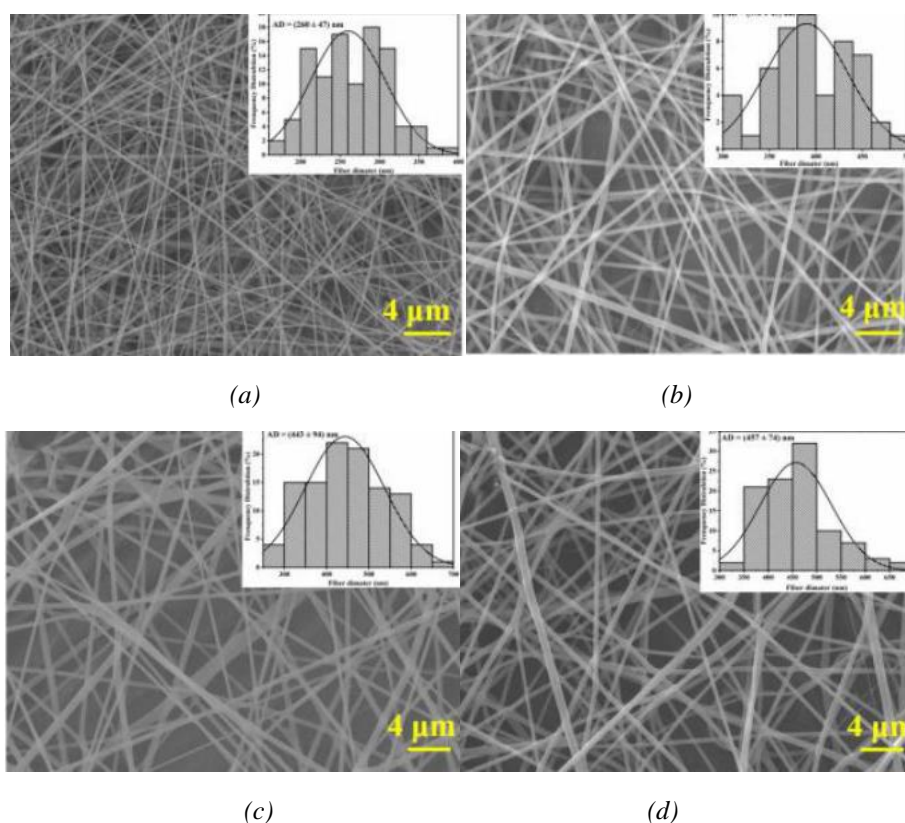


Fig. 2. SEM images and fiber diameter distributions of CS-PEO/PCL fibers at different injection velocity ratios. (a) 1:1, (b) 1:2, (c) 1:4, (d) 1:6.

The microstructure of the core-shell nanofibers was visualized by TEM, as shown in Fig. 3. It can be seen that when the injection velocity ratio was 1:1 (a), the boundary between the core layer and the shell layer was unstable, and the shell layer could not completely wrap the core layer to well form the coaxial structure. However, as the injection speed of the shell layer increased, the shell layer became thicker to package the nuclear layer, forming a well-defined core-shell structure. While the injection velocity ratio increased from 1:2, 1:4 to 1:6, both the fiber diameter and the shell thickness improved. The ratio of core layer thickness to shell layer thickness reached 2.06 ± 0.25 , 1.06 ± 0.19 , and 0.52 ± 0.17 , respectively, which formed three representative core-shell structures, named thin-shell structure, core-shell equipartition structure, and thick-shell structure. In summary, CS-PEO/PCL fibers with controllable morphology and microstructure can be prepared finely by adjusting the core-shell injection velocity ratio.

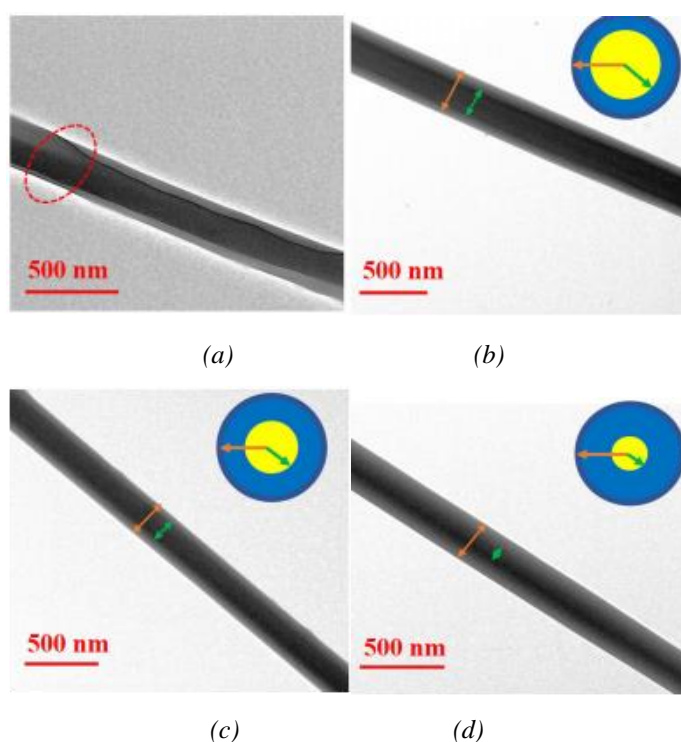


Fig. 3. TEM images of CS-PEO/PCL fibers at different injection velocity ratios. (a) 1:1, (b) 1:2 (thin-shell structure), (c) 1:4 (core-shell equipartition structure) and (d) 1:6 (thick-shell structure).

The dual drug-loaded CS-PEO-Lid/PCL-Cur nanofibers were prepared under the injection velocity ratio of the core layer and shell layer of 1:2, as shown in Fig. 4. From Fig. 4 (a) and (b), it can be seen that the dual drug-loaded nanofibers had the same core-shell morphology and microstructure as the non drug-loaded coaxial nanofibers. The surface of the nanofiber was both smooth and continuous, without the enrichment of drug particles. Compared with the non drug-loaded coaxial nanofibers, the fibers diameter decreased from 390 ± 45 nm to 328 ± 64 nm, and the fibers uniformity decreased slightly as well. This is mainly due to the addition of the drugs increased the conductivity of the spinning fluid, but also made the jet bending instability.

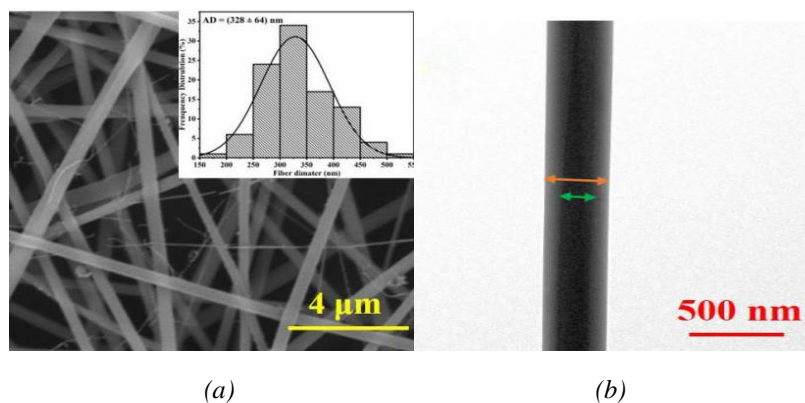


Fig. 4. SEM image and fiber diameter distribution (a) and TEM image (b) of CS-PEO-Lid / PCL-Cur nanofibers.

3.2. Chemical structure and drug molecular distribution

In order to analyze the molecular interactions among the components in the drug-loaded nanofibers, ATR-IR spectroscopy was employed to investigate the nanofiber mats before and after drug loading, as shown in Fig. 5 (a). The broad peak of the CS-PEO nanofiber membrane at 3100-3500 cm^{-1} comes from the overlap of OH...O, -N-H- and the hydrogen bonds in CS molecules; The absorption peaks at 1657 cm^{-1} , 1554 cm^{-1} , and 1152 cm^{-1} are derived from the overlap of the amide I, amide II, and C-O-C [25]. The absorption peaks of PCL electrospun film at 2944 cm^{-1} , 2866 cm^{-1} and 1365 cm^{-1} come from the symmetric and asymmetric stretching and bending vibration of $-\text{CH}_2$. The absorption peak at 1725 cm^{-1} comes from the stretching vibration of carbonyl group; the absorption peaks at 1295 cm^{-1} , 1242 cm^{-1} and 1188 cm^{-1} are mainly from stretching vibration of $-\text{C}-\text{C}-$, $-\text{C}-\text{O}-\text{C}-$ and $-\text{C}-\text{O}-$ [13, 26]. The characteristic absorption peaks of CS-PEO and PCL appeared simultaneously, indicating that the fiber membrane contained these two components. Especially, there are no new absorption peaks in the nanofiber mats after drug loading, which may be caused by two reasons. On the one hand, the drug content in the fiber membrane is low, or the characteristic absorption peaks of the drug and the polymer overlap partly. On the other hand, it also indicates that the drug and the polymer matrix are only mixed without any chemical reaction, and the original properties of the polymer carrier material and the drug can be retained well[27].

X-ray diffraction (XRD) tests were carried out to further investigate the crystallinity of the nanofiber before and after drug loading and the distribution of drug molecules in the nanofiber mats. As shown in Fig. 5 (b), both Lid and Cur drugs have many strong characteristic diffraction peaks, indicating that both the drugs are crystalline substances. The nanofiber membranes showed characteristic diffraction peaks only around $2\theta = 21.4^\circ$ and 23.7° before and after drug loading, indicating that the drugs lost their original crystalline structure after loading into the fiber membrane and were dispersed in the polymer in an amorphous or molecular state[28]. Besides, the diffraction peak intensity of the fiber became weaker after drug loading. This was mainly because the addition of Lid improved the conductivity of the shell solution and accelerated the movement of the shell polymer, thereby prolonging the mutual diffusion time of the shell and the core solutions and inhibiting the crystallization process of PCL [29].

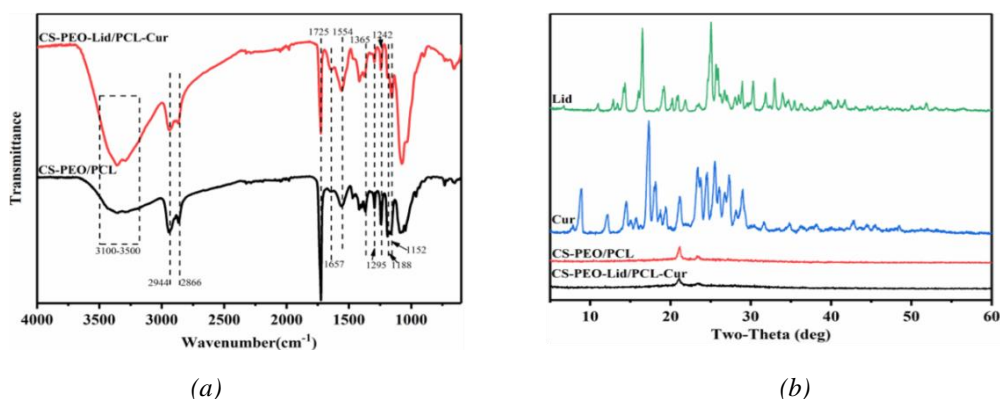


Fig. 5. ATR-IR spectrum (a) and XRD spectrum (b) of coaxial nanofibers.

The distribution of Lid in CS-PEO-Lid/PCL-Cur dual-loaded nanofibers were analyzed by the EDX spectrum. Since the characteristic Cl element is contained in the drug Lid, applying the distribution feature of the Cl element can intuitively reflect the distribution of Lid. As shown in Fig. 6, the Cl element was uniformly distributed in the polymer, which indicated that Lid molecules had a highly dispersed and uniform distribution in the polymer carrier, and the drug had good compatibility with the carrier material.

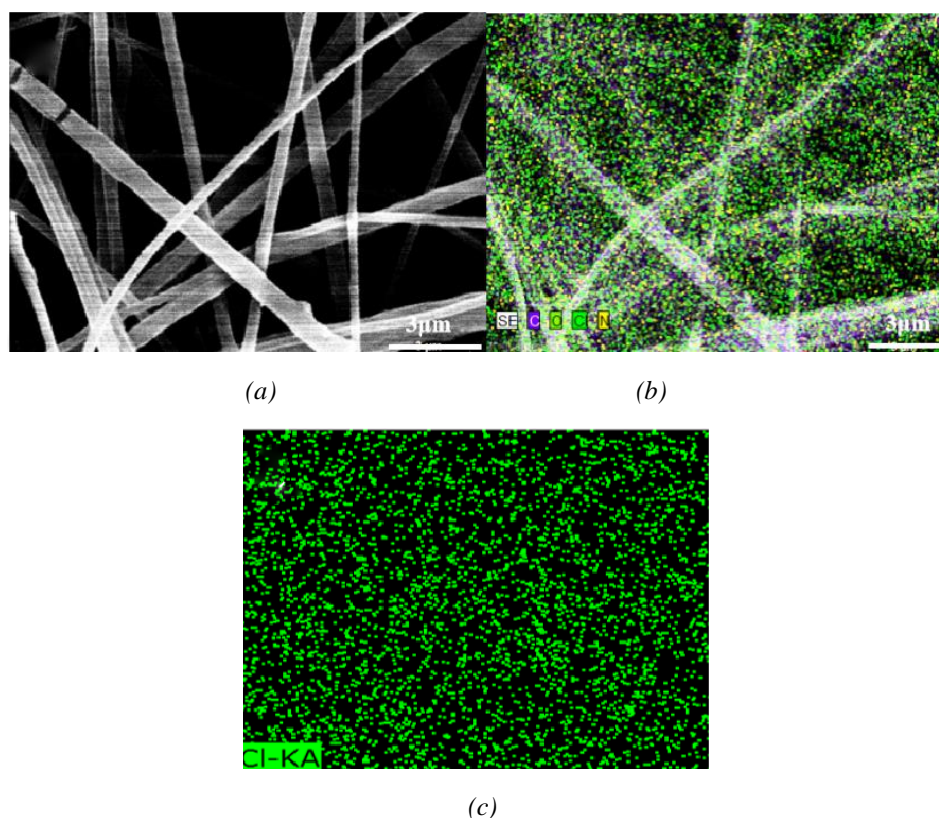


Fig. 6. X-ray element analysis of CS-PEO-Lid/PCL-Cur nanofibers. (a) SEM image, (b) C, O, Cl, N element distribution, (c) Cl element distribution

3.3. In vitro release of the Lid in the shell layer

3.3.1. Lid release of various microstructure nanofibers

Fig. 7 showed the in vitro release curves of Lid in CS-PEO-Lid/PCL nanofibers with injection velocity ratio of 1:2 (thin-shell structure), 1:4 (core-shell equipartition structure) and 1:6 (thick-shell structure) within 72 h. It can be seen that the Lid release curve had the same trend under different injection velocity. As we all know, the Lid, as an analgesic, is required to release quickly and effectively in the early stages of wound formation, which can provide patients analgesic effects in a short time (0.5 h). From the release curves, the release rate of Lid was fast in the first 0.5 h, and the cumulative release rates were 21.58% (1:2), 20.32% (1:4) and 17.74% (1:6), respectively. This is mainly because the Lid molecules could rapidly dissolve out of the fiber surface and reach the affected area when the nanofiber mat was exposed to the PBS buffer (used to simulates approximately wound tissue fluid). In the following 12 h, the cumulative release rate of Lid reached 54.21% (1:2), 49.44% (1:4) and 46.35% (1:6), separately. Thus, Lid could provide a continuous analgesic effect in 12 h. However, the Lid release tended to be gentle in the following

72 h, and the cumulative release rates reached 57.30% (1:2), 53.64% (1:4), and 50.17% (1:6). During this time, the wound was basically in a mild pain state of anti-inflammatory and antibacterial.

Besides, comparing the drug release under three different injection velocity ratios, when the injection velocity ratio was 1:2, both the release rate and cumulative release rate of Lid were the maximum. This is because CS-PEO-Lid / PCL nanofibers had a thinner shell and a larger specific surface area, which could contact more PBS media to accelerate the drug dissolution. Then, as the injection velocity ratio increased, the Lid release from the shell layer of the nanofibers decreased gradually. Therefore, it can be concluded that adjusting the fiber shell thickness can control the Lid release quantitatively, which is expected to be applied to wounds with different pain senses.

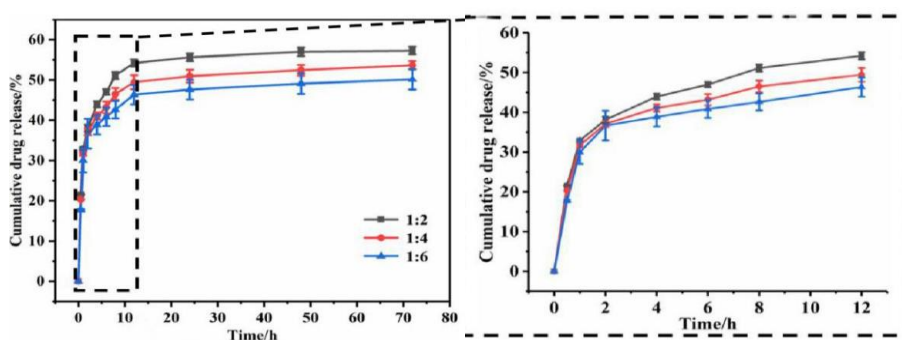


Fig. 7. In vitro release curves of Lid in CS-PEO-Lid / PCL nanofibers with different injection velocity ratios.

3.3.2. Lid release mechanism in the shell layer

The Peppas release model (Equation 1) was used to study the release mechanism of Lid, as shown in Fig. 8 (a), (b) and (c).

$$\frac{M_t}{M_\infty} = kt^n \quad (1)$$

where M_t is the mass of drug released at time t ; M_∞ is the mass of drug released when time is infinite; k is a constant, representing the structure and geometric characteristics of the release system; n is a release index, used to characterize the drug release mechanism.

It was calculated that the release index n of Lid in CS-PEO-Lid/PCL nanofibers with the injection velocity ratios of 1:2, 1:4 and 1:6, was 0.16 (< 0.45), 0.17 (< 0.45) and 0.17 (< 0.45), respectively. Which indicated that the Lid release in the shell layer of the nanofibers primarily via Fick diffusion [30]. The drug concentration difference between fiber and release medium is the main driving force of Lid release [31].

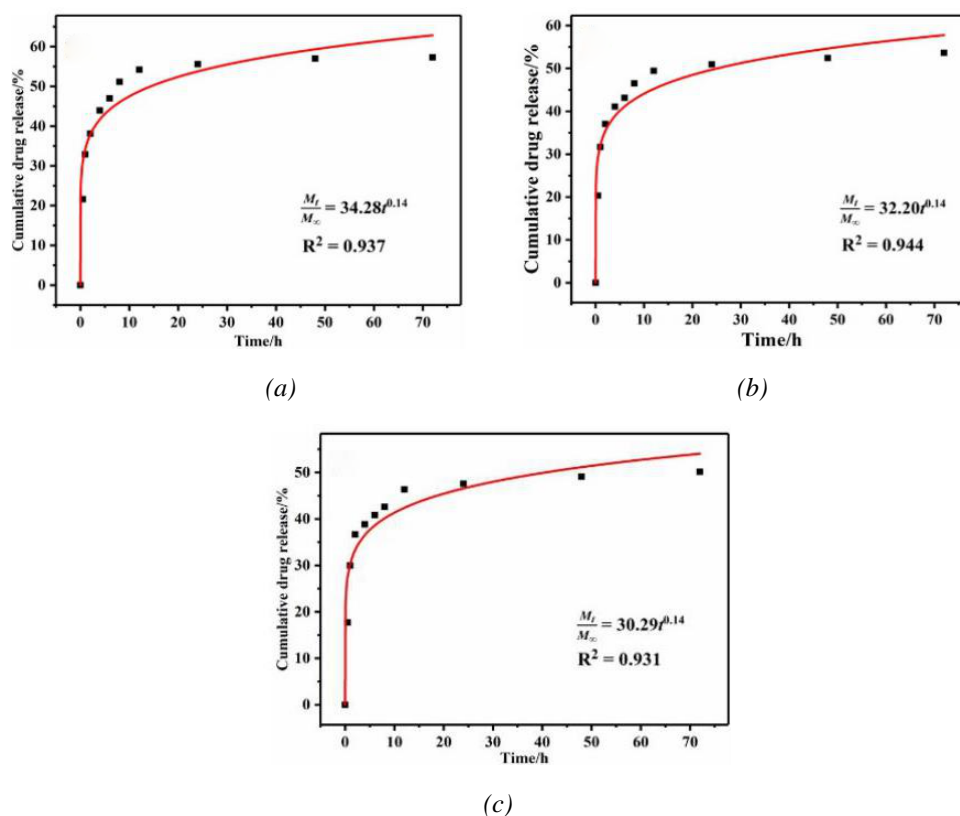


Fig. 8. Lid release kinetics model fitting with the injection velocity ratios of (a) 1:2, (b) 1:4, and (c) 1:6.

3.4. In vitro release of the Cur in the core layer

3.4.1. Cur release of various microstructure nanofibers

Cur, as an antibacterial drug, plays an important role to resistant bacteria and eliminate inflammation. The peak period of acute wound inflammation occurs 2-3 days after the wound formation, and the inflammation lasts for about a week. The persistence of inflammation in chronic wounds is mainly determined by the success of early anti-inflammatory treatment of acute wounds[32]. Therefore, the antibacterial function of wound dressing is particularly important in the first 12 to 72 hours since wound formation, and it is required to achieve the sustained antibacterial effect in the subsequent 168 h.

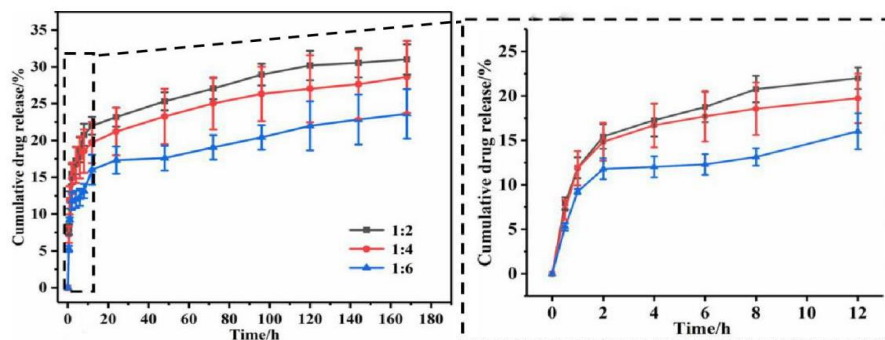


Fig. 9. In vitro release curves of Cur in CS-PEO / PCL-Cur nanofibers with different injection velocity ratios.

Fig. 9 indicated that the Cur release curves had the same trend at different injection velocity ratios. In the first 0.5 h, the cumulative release rate of Cur was 7.90% (1:2), 7.22% (1:4), and 5.28% (1:6), respectively, which was much less than that of Lid in the shell layer at same time. Therefore, loading drugs in the core layer of the nanofibers could avoid effectively drug the sudden release at the early wound stage. Within 12 h, the cumulative release rate of Cur gradually increased, reaching 21.99% (1:2), 19.72% (1:4), and 16.02% (1:6), respectively. Generally, the wound inflammatory response reached the peak within 72h. At this time, the cumulative release rate of Cur was 27.05% (1:2), 25.04% (1:4) and 19.07% (1:6), respectively.

Besides, when the injection velocity ratio was 1:2, both the core-drug release rate and cumulative release rate were the highest, compared with the injection velocity ratios of 1:4 and 1:6. It may be due to the decrease of fiber diameter and shell thickness to supply the shortest path for Cur release from the nuclear layer of the fiber. Therefore, depending on the severity of wound infection, drug-loaded nanofibers with different injection velocity ratios can be selected to control the release amount and release rate of the antibacterial drug.

3.4.2. Cur release mechanism in the core layer

The Peppas release model (Equation 1) was used to study the release mechanism of Cur. As shown in Fig. 10 (a), (b) and (c), the release index of Cur in the three drug-loaded nanofiber mats was 0.17 (<0.45), 0.17 (<0.45) and 0.18 (<0.45), respectively. It showed that the Cur released from the core layer of the nanofiber was also primarily via Fick diffusion, and the drug concentration difference between the nanofiber and the release medium was the main driving source.

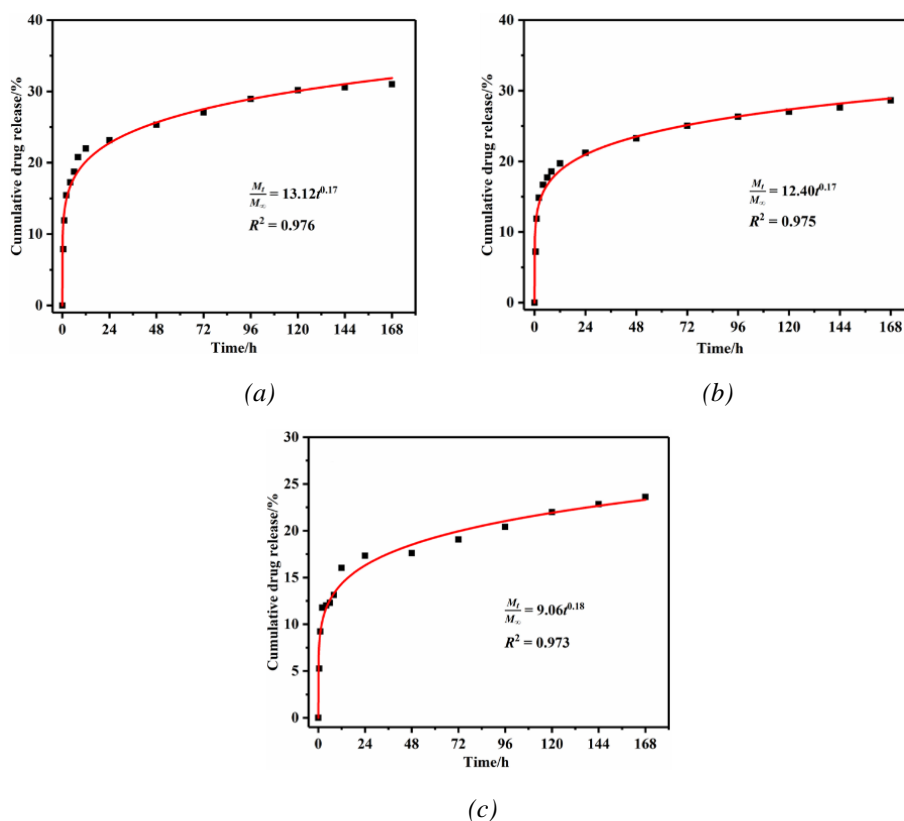


Fig. 10 Cur release kinetics model fitting with the injection velocity ratios of (a) 1:2, (b) 1:4, and (c) 1:6.

3.5. Uniaxial release and biaxial release of Cur

In order to investigate the influence of coaxial structure on the Cur release further, The Cur release behavior in biaxial CS-PEO/PCL-Cur nanofiber with the injection velocity ratio of 1:2 was compared with it in uniaxial PCL-Cur nanofiber, as shown in Fig. 11. It showed that in the first 0.5 h, the cumulative release rate of Cur in CS-PEO/PCL-Cur mat and PCL-Cur mat was 7.90% and 26.03%, respectively. At 12 h, the cumulative release rate of Cur in CS-PEO/PCL-Cur mat and PCL-Cur mat reached 21.99% and 57.96%, respectively. After that, Cur had continued to release in both fibers. At 168 h, the cumulative release rate of Cur in the single-layer structure was still much higher than that in the coaxial structure, which was 81.73 % and 31.01% separately. It can be considered that the multistage structure effectively slowed down the initial release rate of drugs, but also inhibited the total amount of sustained-release. This is mainly because, in uniaxial fibers, the PBS can directly penetrate the drug layer to dissolve and dilute the drug. However, in coaxial fibers, CS-PEO, the shell layer can delay the PBS from penetrating the core layer, reducing the core-drug release rate.

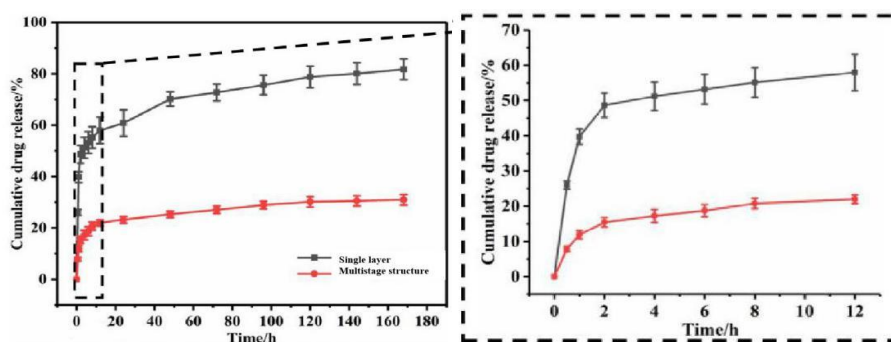


Fig. 11. *In vitro* release curves of Cur in CS-PEO / PCL-Cur and PCL-Cur nanofibers.

4. Conclusions

In this study, by controlling the core-shell injection velocity ratio, we successfully prepared coaxial nanofibers of three representative structures, which were thin-shell structure, core-shell equipartition structure, and thick-shell structure. Addition the drugs in the shell layer or the core layer of the fibers would increase the conductivity of spinning fluid so that the diameter of the fibers decreased slightly. However, the drug-loaded nanofibers still had a clear core-shell structure without the drug particles accumulating, and the mixing between the drugs and polymer matrix was only in a physical form.

In vitro release tests showed that both the release of Lid and Cur was via Fick diffusion, and the drug concentration difference between fibers and release medium was the main driving force. Among the three kinds of core-shell nanofiber mats, because the fibers with injection velocity ratio of 1:2 had, thinner shell, and larger specific surface area, the fiber could absorb more PBS to accelerate the dissolution release of Lid in the shell layer. Meanwhile, to the thin-shell nanofibers, the closest distance of the release medium to the core layer made the release ratio of Cur in the core layer highest. When the injection velocity ratio is 1:2, the Lid in the shell could

rapidly release to 21.58% in the first 0.5h of the wound formation, giving fast relief for the pain. The cumulative release rate could reach 54.21% within 12 h, which achieved sustained pain relief. The cumulative release rate of Cur was only 7.9% in the first 0.5h, and after 12h, it gradually increased, which played a long-acting antibacterial effect.

In conclusion, the sequential release of different drugs in the core-shell structure can be regulated by controlling the fiber injection velocity ratio in subsequent studies. It is expected to overcome the sudden and massive release of drug in uniaxial drug-loaded nanofibers and effectively prolong the release time of the drug in the nuclear layer, forming the time difference of drug release between the core and shell layers.

Acknowledgements

This work was supported by the “Trauma Repair Project” of Action Plan for Science and Technology in Major Disease Prevention and Control from National Health and Family Planning Commission (No. 2017ZX01001).

References

- [1] X. Feng, J. Li, X. Zhang, T. Liu, J. Ding, X. Chen, *Journal of Controlled Release* **302**, 19 (2019).
- [2] D. Han, M. Sasaki, H. Yoshino, S. Kofuji, A. Sasaki, A. Steckl, *Journal of Drug Delivery Science & Technology* **40**, 45 (2017).
- [3] B. Steffansen, S. Herping, *International Journal of Pharmaceutics* **364**(1), 150 (2008).
- [4] L. Vinklárková, R. Masteiková, D. Vetchý, P. Doležel, J. Bernatoniènè, *Biomed Research International* **2015**, 11 (2015).
- [5] T. Maver, U. Maver, F. Mostegel, T. Griesser, S. Spirk, D. M. Smrke, K. S.Kleinschek, *Cellulose* **22**(1), 749 (2015).
- [6] Y. Li, H. Jiang, K. Zhu, *Journal of Materials Science: Materials in Medicine* **19**(2), 827 (2008).
- [7] P. Wen, K. Feng, H. Yang, X. Huang, M. H. Zong, W. Y. Lou, N. Li, H. Wu, *Carbohydrate Polymers* **169**, 157 (2017).
- [8] H. L. Jiang, Y. Q. Hu, Y. Li, P. C. Zhao, K. Zhu, W. Chen, *Journal of Controlled Release* **108**(2-3), 237 (2005).
- [9] C. Y. Wang, W. X. Hou, X. R. Guo, J. H. Li, T. Hu, M. L. Qiu, S. Liu, X. M. Mo, X. D. Liu, *Mater Sci Eng C Mater Biol Appl* **79**, 507 (2017).
- [10] A. Schneider, X. Y. Wang, D. L. Kaplan, J. A. Garlick, C. Egles, *Acta Biomaterialia* **5**(7), 2570 (2009).
- [11] Z. N. Cao, X. G. Luo, H. Zhang, Z. Fu, Z. Shen, N. Cai, Y. N. Xue, F. Q. Yu, *Cellulose* **23**(2), 1349 (2016).
- [12] S. M. Jung, G. H. Yoon, H. C. Lee, H. S. Shin, *Journal of Biomaterials Science Polymer Edition* **26**(4), 252 (2015).
- [13] F. Cheng, J. Gao, L. Wang, X. Y. Hu, *J. Appl. Polym. Sci.* **132**(24), 42060 (2015).

- [14] S. T. Yohe, V. L. M. Herrera, Y. L. Colson, M. W. Grinstaff, *Journal of Controlled Release* **162**(1), 92 (2012).
- [15] X. L. Liu, L. H. Nielsen, S. N. Kodzińska, H. M. Nielsen, H. Y. Qu, L. P. Christensen, J. Rantanen, M. S. Yang, *European Journal of Pharmaceutics and Biopharmaceutics* **123**, 42 (2018).
- [16] L. Fan, C. Cheng, Y. B. Qiao, F. Li, W. Li, H. Wu, B. Ren, *Plos One* **8**(7), 1 (2013).
- [17] X. L. Xu, X. L. Zhuang, X. S. Chen, X. R. Wang, L. X. Yang, X. B. Jing, *Macromolecular Rapid Communications* **27**(19), 1637 (2006).
- [18] B. Xia, Y. Lv, *Materials Science & Engineering* **82**, 253 (2018).
- [19] M. He, H. Y. Jiang, R. Wang, Y. Xie, C. S. Zhao, *Journal of Colloid & Interface Science* **490**, 270 (2017).
- [20] Q. Q. Sang, H. Y. Li, W. Gareth, H. L. Wu, L. M. Zhu, *Journal of Biomaterials Applications* **32**(8), 1105 (2018).
- [21] S. B. Rao, C. P. Sharma, *Journal of Biomedical Materials Research* **34**(1), 21 (1997).
- [22] A. K. Azad, N. Sermsintham, S. Chandkrachang, and W. F. Stevens, *Journal of Biomedical Materials Research* **69**(2), 216 (2004).
- [23] T. Maver, M. Kurečić, D. M. Smrke, K. S. Kleinschek, U. Maver, *Journal of Sol Gel Science & Technology* **79**(3), 1 (2015).
- [24] M. F. Dzikri, T. P. Armedya, S. Q. Khairunisa, S. C. W. Sakti, Y. Raharjo, W. Purnamasari, N. Nasronudin, M. Z. Fahmi, *Digest Journal of Nanomaterials and Biostructures* **14**(1), 203 (2019).
- [25] K. J. Pawlowski, C. P. Barnes, E. D. Boland, G. E. Wnek, G. L. Bowlin, *Mrs Proceedings* **827**, 17 (2004).
- [26] A. K. Haghi, M. Akbari, *Physica Status Solidi* **204**(6), 1830 (2007).
- [27] H. W. Guo, S. J. Tan, J. Gao, L. Wang, *J. Mater. Chem. B* **8**, 1759 (2020).
- [28] E. M. Abdelrazeka, A. M. Hezmab, A. El-khodarya, A. M. Elzayata, *Egyptian Journal of Basic and Applied Sciences* **3**(1), 10 (2016).
- [29] B. Poornima, and P. S. Korrapati, *Carbohydrate Polymers* **157**, 1741 (2016).
- [30] E. Zussman, A. Theron, A. L. Yarin, *Applied Physics Letters* **82**(6), 973 (2006).
- [31] L. H. Wang, H. Yang, J. Z. Hou, and W. X. Zhang, *New Journal of Chemistry* **41**(2), 15072 (2017).
- [32] N. I. Cuello, V. R. Elías, S. N. Mendieta, M. Longhi, M. E. Crivello, M. I. Oliva, G. A. Eimer, *Materials Science and Engineering: C* **78**, 674 (2017).